ACS Biomaterials SCIENCE & ENGINEERING
Article
pubs.acs.org/journal/abseba

Wet Spinning and Drawing of Human Recombinant Collagen

Amit Yaari,[†] Yaelle Schilt,[‡] Carmen Tamburu,[‡] Uri Raviv,[‡] and Oded Shoseyov*[,†,§]

[†]The Robert H. Smith Faculty of Agriculture, Food and Environment, and the Center for Nanoscience and Nanotechnology, The Hebrew University of Jerusalem, P.O. Box 12, Jerusalem, Israel

[‡]Institute of Chemistry and the Center for Nanoscience and Nanotechnology, The Hebrew University of Jerusalem, Jerusalem 91904, Israel

[§]CollPlant Ltd. 3 Sapir Street, P.O. Box 4132, Ness-Ziona, Israel

Supporting Information

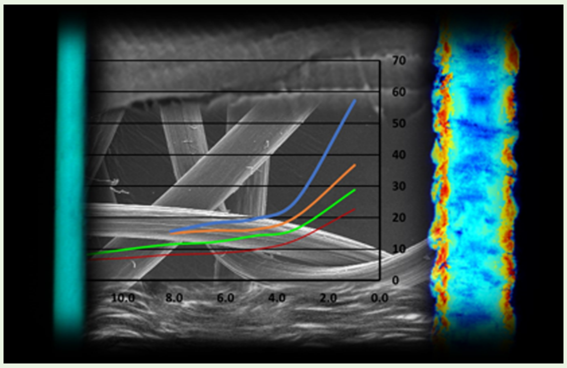

ABSTRACT: The advancement of tissue engineering and regenerative medicine has generated a growing demand for collagen fibers that both resemble native collagen fibers as closely as possible in terms of structure and function, and can be produced in large quantities and processed by current textile technologies. However, the collagen spinning methodologies reported thus far have not matured sufficiently to provide a spinning rate suitable for large-scale production and also generate fibers with insufficient mechanical properties. In the current study, we introduce three new elements into existing collagen fiber spinning technologies: the use of recombinant human collagen, high concentration dope, and spin drawing. At the optimal draw ratio, mechanically strong, aligned, thin fibers, with diameters similar to those of cotton or polyester fibers, are obtained at rates exceeding 1,000 m/h. The resulting fibers display an ultimate tensile strength (UTS) of 150 MPa and a strain of 0.21 after being hydrated in PBS, values which are comparable to and even surpass those reported for human patellar and Achilles tendons. The production technology is simple, based entirely on existing fiber production machinery, and suitable for scale-up and rapid production of large fiber quantities.

KEYWORDS: *recombinant human collagen, wet spinning, fiber, biotextile*

1. INTRODUCTION

As part of the advancements in the fields of tissue engineering and regenerative medicine, a rise in the number of fiber-based and fiber-containing scaffolds has been observed. Designers of such scaffolds often endeavor to mimic the natural structure of the extracellular matrix (ECM), which is fibrillar in nature.[1] Another motivation for the use of fibers is their ability to be processed into a vast array of "biotextile" scaffolds using established techniques developed by the textile industry, such as knitting,[2] braiding,[3] and weaving.[4] These technologies can be used to tailor the scaffolds' mechanical and structural properties, such as extensibility, directionality, density, and porosity.

Many synthetic polymer fibers are available for scaffold production, but even when they possess appropriate mechanical properties, they often lack the ability to communicate with and integrate into the surrounding tissues and consequently evoke inflammation and foreign body response. Therefore, a need still exists for fibers that are both mechanically robust and biocompatible in the targeted biological environment, as well as capable of supporting and guiding cell proliferation and differentiation.[5]

The obvious candidate for a starting material for the production of such fibers is type I collagen, which is the major fibrillar constituent of the ECM, particularly in load-bearing tissue. Production of pure collagen fibers by extrusion- or wet spinning-based methodologies has been reported and was first patented over 50 years ago.[6] In the vast majority of past reports, the starting material comprised a collagen solution or dispersion, typically at pH 2−3 and at concentrations between 0.1−1%. This solution is then injected (the term extruded is sometimes used) through a small orifice (termed a "die" or a "spinneret") into a coagulation bath. Different solutions or organic solvents are employed as coagulants, but the purpose remains the same: to dry and neutralize the collagen solution/dispersion and thus induce fibrillogenesis and precipitate the collagen into a solid fiber. The fibers are then cross-linked by a chemical or physical cross-linking method to strengthen and stabilize them. The same principal elements (i.e., injection of a protein solution through a spinneret, fibrillogenesis by means of pH control and dehydration, and finally cross-linking) can be traced back to the natural fiber spinning processes, as performed by spiders[7] and silk worm[8] to produce silk fibers, and by collagenous tissue morphogenesis

Received: November 2, 2015
Accepted: February 15, 2016
Published: February 15, 2016

DOI: 10.1021/acsbiomaterials.5b00461
ACS Biomater. Sci. Eng. 2016, 2, 349−360

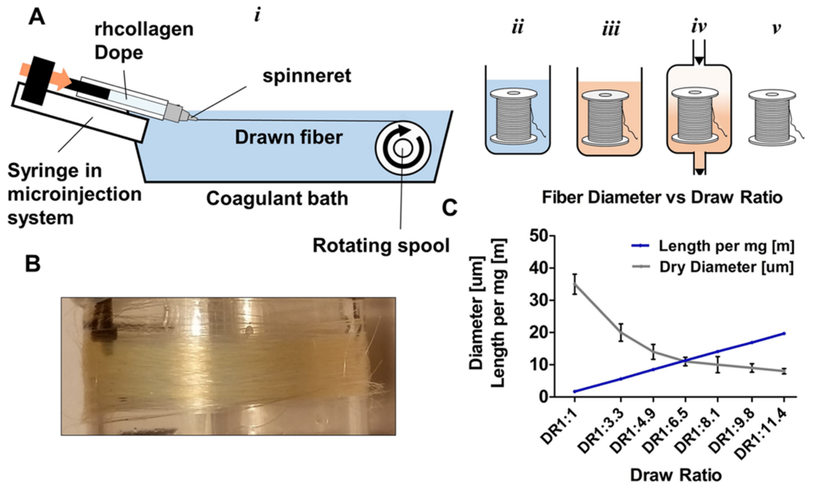

Figure 1. Wet spinning and drawing system. (A) Setting of the wet spinning and drawing system and fiber formation process. (i) A syringe fitted in a microinjection system injects the rhcollagen dope through a small bore ceramic spinneret into a coagulation bath. A speed-controlled rotating spool collects the fiber at the desired take-up speed. The ratio between the injection and take-up velocities determines the draw ratio (DR). (ii) The fiber, wound on the spool, is cross-linked and washed, (iii) dehydrated in ethanol, and (iv) dried by a critical point drying process in CO_2, to yield (v) dried finished fibers. (B) An image of a GTA-cross-linked dehydrated fiber sample. (C) A plot of fiber diameter (gray) and the length (in meters) per mg rhcollagen vs draw ratio.

processes, such as the selachian egg case generation process[9] and mussel byssus thread formation.[10] However, two critically important elements employed in the natural spinning processes are omitted in most of the aforementioned studies of reconstituted collagen fiber spinning systems and methods: liquid crystalline (mesophase) alignment and drawing. Natural spinning processes meticulously control the pH, ionic composition, and concentration of the protein monomers inside their spinning duct, to induce the formation of liquid crystalline dope, which can then be efficiently aligned in the direction of the fiber axis upon application of shear force. During the last stages of its passage through the spinning duct and immediately upon exit from the spinneret, the semisolid dope is drawn, forcing the monomers to slide past each other and further align in the direction of the fiber axis. This step is critical for fiber structure, order formation, and development of robust mechanical properties.[11]

In this work, recombinant human type I collagen (rhcollagen) is applied in a novel collagen fiber spinning method. The rhcollagen is produced from a transgenic tobacco plant that expresses two human genes encoding recombinant heterotrimeric collagen type I (COL alfaI and COL alfaII), along with the three human post translational modifying genes, human prolyl-4-hydroxylase (P4H alfa and P4H beta) and lysyl hydroxylase 3 (LH3) enzyme genes.[12] After purification, correctly folded and fully functional human recombinant collagen heterotrimers are obtained (rhCOL). In addition to being safe from human pathogens, the rhcollagen is highly hydrophilic and free of high molecular weight forms, which are typically found in tissue extracted collagen, making rhcollagen suitable for the preparation of high concentration homogeneous solutions.

Herein, we present a new method for spinning collagen fibers from Type I rhcollagen, using a novel combination of spin-drawing and relatively high concentration dopes. The structure and mechanical properties of the spun rhcollagen fibers are characterized, and the effect of draw ratio is discussed. In addition, their ability to guide the alignment of rat tenocytes is assessed *in vitro*.

2. MATERIALS AND METHODS

2.1. Collagen Source. Recombinant human atelocollagen (“Collage”, 3 mg/mL in 10 mM HCl) was kindly provided by Collplant Ltd. (Nes-Ziona, Israel).

2.2. Reagents. Except where otherwise noted, all reagents were purchased from Sigma-Aldrich Ltd. (Rehovot, Israel).

2.3. Collagen Dope. The collagen solution was concentrated to 30 mg/mL by dialysis in a dialysis bag (molecular weight cutoff of 3.5 kDa, “SnakeSkin” Thermo Fisher Scientific) against 10% polyethylene glycol (molecular weight 35 kDa) in 10 mM HCl (pH 2). Before spinning, the dope was centrifuged at 4,000 RCF for 5 min to remove gas bubbles.

2.4. Fiber Wet Spinning. The wet spinning and drawing apparatus (Figure 1-A(i)) comprised an injection system, a coagulation bath, and speed-controlled collecting mandrel (spool). The acidic rhcollagen dope was placed in a plastic syringe to which a ceramic die was fitted. In order to produce fibers comparable in diameter to cotton or textile polymer fibers (10−15 μm), a modified ceramic capillary (Kulicke & Soffa, 48FFA-4146-R31) was used, with an internal 10° conical taper and 30 μm orifice diameter. Use of smaller diameter dies resulted in frequent clogging and necessitated high injection pressures, and was therefore avoided.

The syringe was placed in a Chemyx “Nanojet” microinjection system, with volume, time, and injection rate controls. The dope coagulated immediately upon exposure to the coagulant and formed a soft but solid fiber that was able to support its own weight for lengths up to 1.5 m.

After exiting the spinneret, the fiber traveled a distance of 15 cm inside the coagulant and was then rolled up onto a rotating spool placed inside the coagulation bath. The spool was attached directly to a Heidolph “RZR 2052” controlled stirrer which was used to determine its rotation speed. Fiber linear take-up speed (collection rate) in m/s was calculated by multiplying the spool’s circumference by its rotation speed (in RPM). In order to prevent fiber breakage, the injection angle (the angle at which the fiber exits the spinneret) was kept as small as possible. As soon as the fiber emerged from the spinneret, it was picked up using tweezers and wound onto the rotating spool for collection. The injection flow rate of the dope was kept constant at 30 μL/min, giving a fiber production rate of 0.026 m/s at the exit from the spinneret. In order to produce undrawn fibers, injection and take-up speeds were equilibrated (hence, draw ratio 1:1 (DR1:1), i.e., the take-up speed was maintained at 0.026 m/s, leaving a free-floating fiber section between the spinneret and the spool. To introduce drawing, the take-up speed was increased, while the injection rate was maintained constant. To obtain a DR of 1:2, for example, the take-up speed was set to 0.052 m/s. Fibers were injected at 7 different draw ratios: DR 1:1, 1:3.3, 1:4.9, 1:6.5, 1:8.1, 1:9.8, and 1:11.4. The maximum take-up speed that was stably achieved was 0.295 m/s at DR 1:11.4.

After spinning, the fibers, wound on the spool, were incubated in the coagulation buffer (Figure 1A(ii)) for 24 h to ensure neutralization of the dope. The coagulation buffer comprised phosphate buffered saline (PBS), 10 mM phosphate, 2.7 mM KCl, and 0.137 M NaCl at pH 7.4, to which 2 M NaCl was added.

Two cross-linking methods were tested: glutaraldehyde (GTA) for maximal mechanical performance and sustainability, and EDC/NHS, for fibers to be used in cell culture. Either 0.1% glutaraldehyde or 50 mM 1-ethyl-3-(3-(dimethylamino)propyl) carbodiimide (EDC) and 100 mM *N*-hydroxysuccinimide (NHS) were added directly to the coagulation buffer followed by further 24 h of incubation at room temperature. After cross-linking, the fibers were rinsed three times in purified water to remove the cross-linker and salt residues.

For drying, the fibers were gradually dehydrated by 2-h incubations in solutions of increasing ethanol concentrations (50%, 75%, 87% 95%, and 100%) (Figure 1A(iii)). After dehydration, the fibers were dried by a critical point drying process (Figure 1A(iv)) to prevent fusion of their outer surfaces as a result of water adhesion forces. At least 15 m was produced from each draw ratio. The dried, finished fibers (Figure 1A(v)) were kept at room temperature for further testing.

2.5. Critical Point Drying. CPD was performed on a Quorum Technologies k850 critical point dryer. Fibers on spools were removed from 100% ethanol and introduced into the CPD chamber, precooled to 5 °C. After sealing the chamber, the ethanol was exchanged with liquid CO_2. This was performed by filling the chamber with the liquefied gas, rinsing for 2 min, and then emptying the chamber and refilling with fresh gas; the process was repeated three times or until no ethanol was detected in the exhaust gases. The chamber was filled again, and the temperature was increased to 32 °C, a temperature at which CO_2 undergoes sublimation, reaching a pressure of 1,150 PSI. The pressure was then gradually released, taking heed not to lower more than 100 PSI/min.

2.6. Mechanical Characterization. Tensile testing of the fibers was performed on an Instron model 3345 machine equipped with the "Bluehill Lite" analysis software. A Honeywell model 31 low load cell, with a 50 g load range was used. The load cell was calibrated with a 20 g standard weight before each test session. Testing was performed at a 2 mm/min rate.

At least 15 m of fiber was produced for each draw ratio, from which five 50 mm samples were chosen at random. Fiber samples were well affixed in a 1 mm-thick polypropylene frame between two layers of double-sided tape; tests were performed to confirm that no slippage occurred. The fiber samples were positioned so that at least 1 cm ran through the tape on each side of the sample, and the tested region was 20 mm long. For wet testing, the fiber was dipped into PBS for 3 h before the test.

Fiber diameter and sample length were input to the Bluehill software, which generated the stress−strain graphs, ultimate tensile strength (UTS), extension, energy at break, and Young's modulus data. Prior to testing, the diameter of every fiber sample was determined by a Nikon eclipse 80i microscope, fitted with an Abrio CRI system for imaging and analysis (see below).

2.7. Swelling Test. To quantitate fiber swelling, five fiber samples, each measuring 30 mm long, were randomly chosen from different regions of a long (>20 m) fiber spool. Dry fiber diameters were determined at 5 points along the fiber with the aid of a Nikon eclipse 80i microscope, fitted with an Abrio CRI system for imaging and analysis (see below). The fiber samples were rehydrated in PBS for 3 h, and the diameter was remeasured. The swelling percent was calculated as ((wet diameter − dry diameter)/dry diameter) × 100.

2.8. Scanning Electron Microscopy (SEM). Dry fiber samples were placed on an aluminum stub using carbon tape and then coated with Au/Pd in a high-vacuum coater for 60 s with a 2 A current. The estimated coating thickness was 3 nm. SEM was performed with an FEI "Sirion" microscope.

2.9. Polarized Light Microscopy and Image Analysis. Polarized microscopy was performed with a Nikon eclipse 80i microscope, fitted with an Abrio system (CRI, Germany) for polarized imaging and analysis.[13] The optical system includes a CCD camera, liquid-crystal (LC) compensator optic, and a circular polarizer/interference filter optic (CP/IF). Image acquisition and analysis were performed using the Abrio 2.2 software. Background and specimen images were captured under identical conditions (546 nm).

2.10. Construction of the Scaffold for Cell Culture. EDC/NHS cross-linked fibers were stretched over glass coverslips measuring 24 × 20 × 0.1 mm, previously treated with "sigmacote" (Sigma-Aldrich) to render them more hydrophobic. Fiber samples were anchored to coverslips on both sides using a drop of silicone adhesive (DOW CORNING 732). This formed a >15 mm fiber section secured between the anchoring points and resting on the treated glass surface. Each coverslip formed an experimental unit that contained six fiber samples, one from every draw ratio. A 2 mm gap was left between the fibers. After curing of the adhesive (room temperature, 24 h), the constructs were placed inside sterile six-well plates and rehydrated for 30 min in ddH_2O and sterilized by overnight incubation in isopropanol. They were then transferred into a new, sterile plate and rinsed 3 times in sterile ddH_2O for 30 min and once in growth medium for 30 min in a 37 °C incubator.

2.11. Rat Tenocyte Isolation. Tenocytes were extracted from rat Achilles tendon according to a previously reported procedure.[14] Briefly, Achilles tendons were dissected from young rats, cut into small pieces, and transferred into a culture flask containing Dulbecco's modified Eagle's medium (DMEM) with 50% fetal calf serum (FCS). After 24 h at 37 °C, an additional 3 mL of DMEM with 50% FCS were added and incubation continued for another 24 h at 37 °C. During the incubation period, tenocytes migrate out of the tissue and adhere to the flask. Following removal of the tissue and old medium, fresh DMEM plus 10% FCS and 1% penicillin−streptomycin (PS) (BIOLAB Ltd., Israel) were added, and the cells were cultivated for 96 h at 37 °C. For subculture, cells were detached via a brief trypsin EDTA (Biological Industries, Israel) treatment and then reseeded.

2.12. Cell Alignment Assay. Cells (100,000 in 1 mL DMEM plus 10% FCS) were spread on the coverslip fiber scaffold in each well and left to adhere for 30 min. Wells were then filled with medium. The plates were incubated in a 5% CO_2 incubator at 37 °C for 72 h. The assay was terminated by aspiration of the medium, and the cells were fixed by the addition of 3% paraformaldehyde (PFA) supplemented with 0.5% triton X-100 for 3 min incubation, followed by a 20 min incubation in 3% PFA at 37 °C. After 3 washes in PBS, 1% skim milk was added as a blocking solution, and samples were incubated for 1 h. DAPI (300 nM) and Pahlloidin (50 nM) (both from Thermo Fisher Scientific) were added, and after 1 h of incubation, the samples were washed 3 times with PBS and then stored in the dark at 4 °C for up to 1 week before imaging.

2.13. Fluorescent Image Acquisition. Imaging of the fluorescently labeled samples was performed with an EVOS 6500-FL fluorescent microscope (Life Technologies). A 20× magnification was used for all sample and control pictures. For imaging the DAPI stained nuclei, 360 nm excitation and 447 nm emission were used. For the Pahlloidin-stained actin fibers, 530 nm excitation and 593 nm emission were used.

2.14. Image Analysis. The "CellProfiler" version 2.1.1 program[15] was used for image analyses. The fluorescent images of the DAPI stain (461 nm) were used as input files. In the first analysis stage, the nuclei were identified as primary objects based on the following parameters: typical object diameter, 20 to 40 pixels; threshold strategy, global; thresholding method, MoG; smoothing method for thresholding, automatic; threshold correction factor, 2; method to distinguish clamped objects, shape; and method to draw dividing lines between clumped objects, intensity. These parameters were selected after multiple iterations and manual verification of accurate identification of the number and shape of nuclei in all experimental groups. The same parameters were used for all experimental groups and controls. In the second analysis stage, the "MeasureObjectSizeShape" module was used. This module assigns the best-fitting ellipse to every identified nucleus, and quantifies the following parameters: "MajorAxisLength", the length (in pixels) of the major axis of the fitted ellipse; area, the actual number of pixels in the identified nucleus image; and orientation, the angle (in degrees ranging from −90° to 90°) between the *x*-axis and the major axis of the fitted ellipse. The fiber axis was set parallel to the *x*-axis (0°).

2.15. Statistical Analysis. Statistical analysis was performed with JMP pro 10 software. One-way analysis of variance (ANOVA) was used for multiple comparisons. For pairwise comparisons, a two sample *t*-test was used. Statistical significance was set at $P < 0.05$. Normality of the populations sampled was assumed. Homogeneity of variances of the populations was verified by Bartlett's and Levene's tests. Numerical data are presented as the mean ± standard deviation (SD). Means and SDs were calculated using Excel software (Microsoft Corporation).

2.16. Differential Scanning Calorimetry (DSC). Fiber samples weighing between 2.0 to 4.0 mg were incubated in PBS for 3 days before testing. The samples were placed in aluminum sample pans, covered with PBS, and sealed. PBS was used as reference, and weights of the reference and sample pans were matched. The temperature range tested was from 5 to 95 °C, at a 5 K/min scan rate. Tests were performed under dynamic nitrogen atmosphere (50 mL/min) on a Shimadzu DSC-50.

3. RESULTS

3.1. Effect of Draw Ratio on Fiber Structure and Morphology. A sample of dried, GTA cross-linked fibers on a spool (spun at DR 1:8.1) is shown at Figure 1B. Fiber diameter sharply decreased with increasing draw ratio (Figure 1C), whereas at DR 1:1 the fiber diameter was 35 μm, at DR 1:8.1 it was reduced to 10 μm, and at the maximal draw ratio of 1:11.4, it was 8 μm. Accordingly, the length spun from 1 mg of protein was increased from 1.7 m at DR1:1 to 19.7 m at DR1:11.4. The fiber production rate was over 760 m/h at DR 1:8.1 and over a 1,000 m/h at DR 1:11.4.

Scanning electron microscopy was employed to characterize fiber morphology. For clarity, throughout this text, "orientation" will be used to describe the property of molecular and fibrillar axes in the direction of the fiber axis across the observed area, whereas "alignment" will be used to describe the property of molecular and fibrillar order, i.e., molecular and fibrillar axes within the same region pointing in the same direction but not necessarily with the fiber axis. The impact of draw ratio on the orientation of the fiber's outer surface was clearly visible. Undrawn fibers (DR 1:1) displayed a very rough surface with deep grooves and pits (Figure 2A), reminiscent of a wrinkled cloth. When drawing was introduced at DR 1:3.3 (Figure 2B), a substantial alteration in the fiber surface was observed. The fiber surface became much smoother and homogeneous; some crevices were observed, but were shallower than those in the undrawn fibers, and most of them were aligned with the fiber axis. As the draw ratio was further increased to DR 1:4.9, the crevices on the fiber surface became even shallower and were almost entirely oriented with the fiber axis. This trend continued throughout all tested draw ratios and culminated with the highest draw ratio (DR 1:11.3) that yielded the smoothest and most homogeneous fibers (Figure 2D−G).

The fractured fiber ends revealed a core−shell structure, in which both components were affected by the draw ratio. Undrawn fibers (DR 1:1, Figure 3A) had a thick shell that appeared to be tightly packed and fused, with a wrinkled morphology. The inner core (Figure 3B) was composed of fine, well-separated fibrils, which formed a wavy pattern (crimp), that were loosely oriented with the fiber axis and had a wavelength of approximately 2 μm. Multiple voids between the fibrils were clearly visible. When the draw ratio was increased to DR 1:4.9, the core−shell structure was still maintained, but the outer shell was thinner (Figure 3C), appeared to be less fused, and was much better aligned and oriented. The core was composed of thin, well-separated fibrils. The fibrils appear to be better aligned (Figure 3D), with greater packing density and smaller voids between them. The crimp pattern was less pronounced and was mainly observed in the center of the core.

In contrast, fibers drawn at the maximal draw ratio, DR1:11.4 featured a uniform, continuous morphology, and no core−shell structure was discerned (Figure 3E). The bulk of the fiber, which appeared fused, broke under pressure (see right side of Figure 3E) revealing highly aligned, highly oriented, and densely packed fibrils.

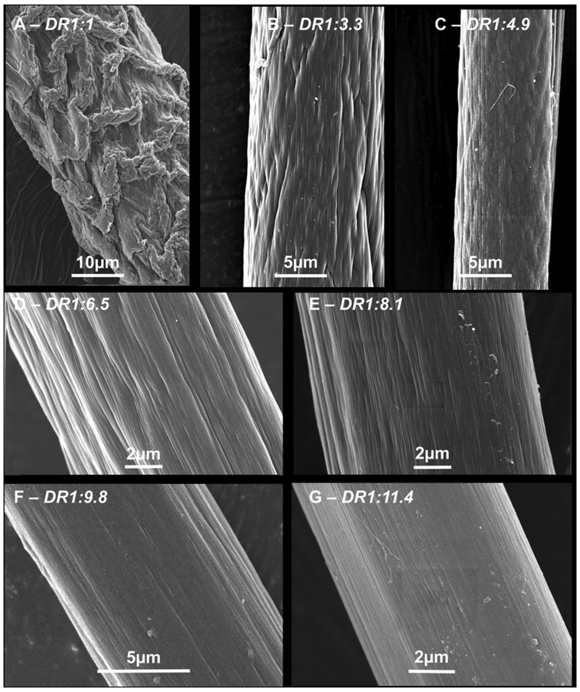

Figure 2. Scanning electron microscopy images of fibers drawn at different draw ratios. A to G: DR1:1, DR1:3.3, DR1:4.9, DR1:6.5, DR1:8.1, DR1:9.8, DR1:11.4, respectively. Note the differences in scale between the various images.

3.2. Effect of Draw Ratio on Order and Alignment. Polarized microscopy is a tool commonly used to characterize the degree of fibrillar order and orientation of collagen samples, as reflected by birefringence and slow optical axis.[16] The wet spun fibers were analyzed by the "Abrio" polarized light microscopy system that quantifies retardance (in nanometers) and determines the orientation azimuth of the slow optical axis of the sample by measuring the relative phase shift between two orthogonally polarized light waves.[13] For collagen, the slow optical axis is aligned with the molecular axis,[16a] and therefore, the given orientations are the molecular and fibrillar orientations of rhcollagen. For imaging purposes, the Abrio software generates a pseudocolor image, where color denotes the orientation of the slow optic axis and the intensity indicates retardance. The retardance is dependent on both the sample thickness and the degree of alignment.

A side-by-side display of fibers spun at different draw ratios is presented in Figure 4. Insets at the top depict the retardance

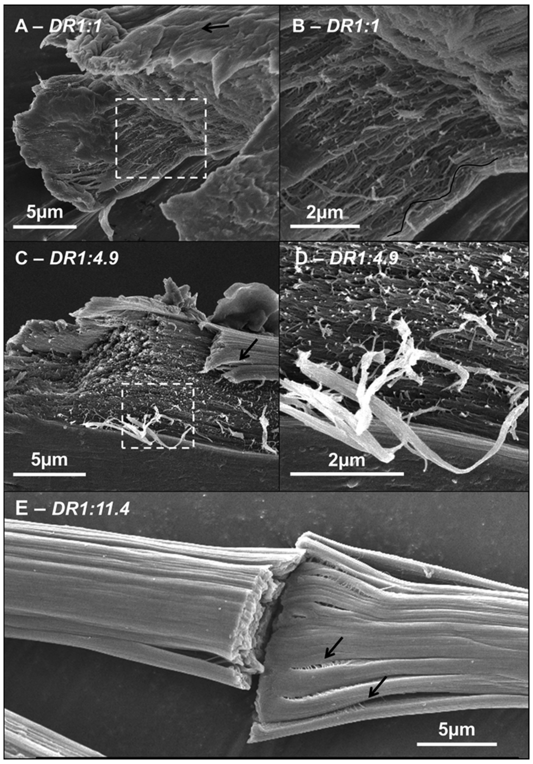

Figure 3. SEM of fractured fiber ends. (A and B) DR 1:1. B is a magnification of the area marked by the broken white line in A. The black arrow denotes the fiber's outer shell. (B) The black wavy line at the bottom right marks the crimp pattern of the fibrils. (C and D) DR1:4.9. A core−shell structure is still visible. The black arrow shows the separation of the shell into its constituent subfibrils. D is a magnification of the area marked by the broken white line in C, showing higher alignment and tighter packing of the core fibrils. (E) DR 1:11.3. Arrows denote areas where the fiber separates into the component subfibrils.

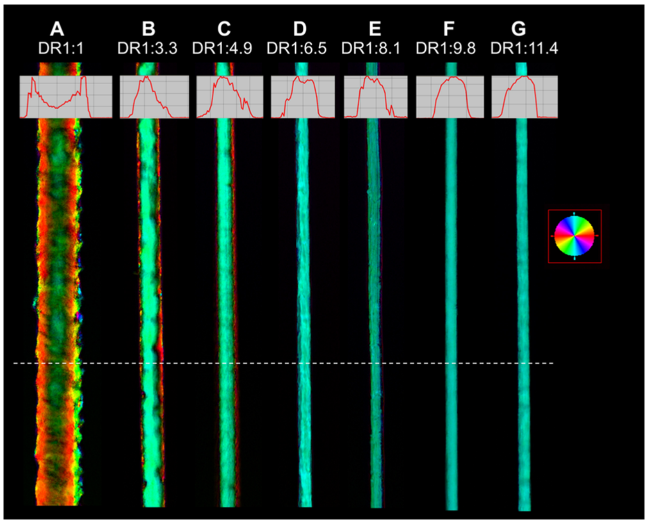

Figure 4. Polarized microscopy of wet spun collagen fibers (20× magnification). Color (see scheme on right) indicates the azimuthal orientation of the slow optical axis (molecular axis), and intensity indicates the degree of retardance (nm). Insets at the top depict the retardance intensity along the white broken line that transverses the fibers perpendicular to their axis. Note that the insets are not to scale with the fiber images but expanded to ease viewing. Fibers spun at the different draw ratios from A to G are DR 1:1, DR 1:3.3, DR 1:4.9, DR 1:6.5, DR 1:8.1, DR 1:9.8, and DR 1:11.4 respectively.

intensity along the white broken line that transverses the fibers perpendicular to their long-axes. Undrawn fibers (DR1:1, Figure 4A) displayed a retardance pattern commensurate with a distinct core−shell structure. The intensity diagram at the top shows that the strongest retardance was recorded at the fiber circumference, and not at its core, where sample thickness was maximal. This pattern suggests a shell with higher fibrillar alignment and density that envelopes a loosely packed core. When looking at a longitudinally cut fiber, a faint cyan region was seen along its center, indicating molecular and fibrillar alignment with the fiber axis. As the light transverses the entire fiber diameter in that region, where core thickness is maximal and shell thickness is minimal, the orientation reflected by the signal was attributed to the core.

When focusing on the area closer to the fiber fringes, where the shell component becomes more significant relative to the core, fibril orientation appeared weaker. Multiple small patches displaying 45° or even 90° fibril orientation relative to the fiber axis were observed. This finding is in agreement with the wrinkled and rough surface observed along the outer shell by SEM.

Fibers drawn at DR 1:3.3 appeared to have a fundamentally different intensity profile (Figure 4B, top), with a maximal retardance measured along their center, at the thickest region, which declined toward the fringes. This indicates that the alignment and density in the core were more substantial relative to the shell, where it only became visible near the fiber fringes, where core thickness was small. The shape of the intensity diagram was not smooth, reflecting the surface roughness observed in the SEM images. Fibrillar alignment was strong, and the fibrils were well oriented with the fiber axis throughout the bulk of the core, as reflected by the dominance of the cyan hue in the fiber center (Figure 4B, body). The core appeared to be forming a faint crimp pattern, with a hue that shifted toward green when kinked right and toward blue when kinked left. In contrast, orientation was lost in the fiber shell, as manifested by multiple color patches, indicating orientations deviating from the fiber axis by as much as 90°.

This trend was maintained in fibers prepared at DR 1:4.9. Fibers displayed a rounder intensity diagram (Figure 4C, top), reflecting further thinning of the nonoriented shell. The fiber core was smoother, with a very weak crimp still visible as small kinks sparsely dispersed throughout (Figure 4C, body). The shell was almost absent, and appeared as a very thin unoriented layer, mainly on the right side of the fiber. At DRs 1:6.5 and 1:8.1 (Figure 4D,E, body), fibers lacked the outer shell altogether and displayed a homogeneously oriented body (only the cyan hue was visible). However, intensity was not uniform, reflecting the presence of some crevices and folds or possible density changes along the fiber axis. DR 1:8.1 and 1:11.4 fibers (Figure 4F,G, top) featured a smooth circular shape, with well-defined edges. The fiber bodies showed both high uniformity and strong alignment of the monomers and fibrils, reflected by the strong intensity and uniform cyan color (Figure 4F,G, body).

In order to quantify and compare the degree of order in fibers spun at the different DRs, their birefringence was calculated and plotted against the draw ratio (see Figure S1). A low level of birefringence was recorded in undrawn fibers (DR 1:1) and was only slightly increased in DR 1:3.3 fibers. A strong rise was observed, however, when DR was further elevated to

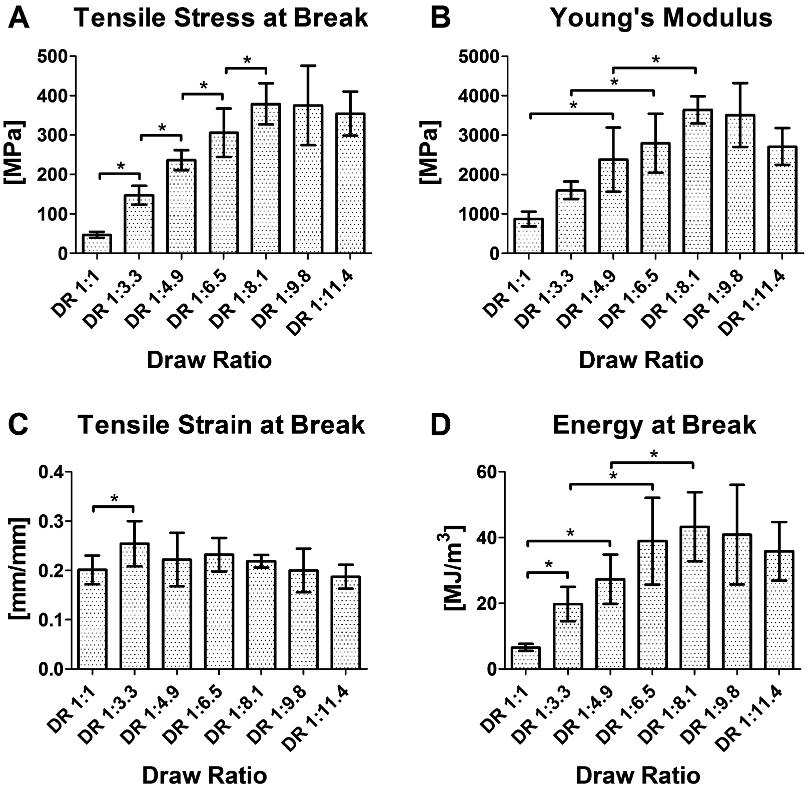

Figure 5. Comparison of UTS, Young's modulus, tensile strain at break, and energy at break between fibers drawn under different draw ratios. Five samples were tested for every draw ratio. (A) Tensile stress at break. (B) Young's modulus. (C) Tensile strain at break. (D) Energy at break. The combined effects of the tensile strain and the UTS graphs are observed. Error bars shows the SD. Asterisks denote the statistical significance of $p < 0.05$.

1:4.9 which formed a local peak. Lower birefringence was then measured for DR 1:6.5 and 8.1 fibers, followed by a strong and steady birefringence increase for the two remaining draw ratios, 1:9.8 and 1:11.l.

3.3. Effect of Drawing on Mechanical Performance. To characterize the effect of fiber draw ratio on the mechanical properties of the drawn fibers, tensile stress and strain performance of the glutaraldehyde cross-linked fibers were assessed (Figure 5). As shown by Figure 5A, fiber UTS increased linearly as DR was increased up to 1:8.3 ($p < 0.05$). After this point, the UTS plateaued and even slightly declined at DR 1:11.4. A similar pattern was observed for the fibers' Young's modulus (Figure 5B), although statistical significance was not detected between each draw ratio increment. It was, however, detected between every second draw ratio. The peak modulus was in DR 1:8.1 fibers, followed by a steeper decline.

Tensile strain at break (Figure 5C) peaked at a draw ratio of 1:3.3 and was larger than that measured for DR 1:1 fibers ($P < 0.05$). No other significant differences in tensile strain at break were measured between fiber groups, but the general trend was of gradual decline with increasing draw ratio.

Fiber toughness (energy at break) is actually a function of the tensile stress and strain and therefore reflects their combined trends. The highest value was obtained at draw ratio 1:8.1, beyond which it gradually decreased (Figure 5D). The steepest incline was observed between DR 1:1 and DR 1:3.1, ascribed to the strain increase between them.

3.4. Cross-Linking. Two cross-linking systems were used: glutaraldehyde (GTA) and 1-ethyl-3-(3-(dimethylamino)-propyl) carbodiimide (EDC). GTA was employed as a cross-linking agent due to its effectiveness, ease of application, and to allow direct comparison to past works. Previous works on collagen fiber spinning have found GTA to give the highest UTS and lowest swelling.[6i,17] However, although it is an effective cross-linker, GTA is cytotoxic[18] and therefore unsuitable for cell culture applications or for applications that require faster biodegradation. For these reasons, we also employed EDC, a cross-linker commonly used and tested for in vivo human use,[19] as a cross-linker to enable cell culture on the drawn fibers.

Fiber swelling was quantified as a measure of fiber cross-linking effectiveness. Figure 6 shows the swelling behavior of GTA cross-linked fibers. Fiber swelling strongly correlated with draw ratio, where fibers formed under high DRs swelled substantially more than those collected under lower DRs. At DR 1:11.4, the fibers swelled by 80%, whereas DR 1:1 fibers swelled by only 20%.

To compare the different cross-linking approaches (i.e., GTA and EDC), fibers drawn at DR 1:8.1 (the draw ratio that yielded the best mechanical performance in the GTA cross-linked fibers) were cross-linked and compared. Figure 7A shows the dry diameter, wet diameter, and swelling percent recorded for DR 1:8.1 fibers cross-linked using either of the two methods. EDC-cross-linked fibers swelled approximately 2-fold more than the GTA-cross-linked fibers ($P < 0.01$). No significant difference in fiber extension at break was observed between the different cross-linking treatments or hydration states (Figure 7B). The dry fiber stress at break was approximately 20% lower for dry EDC-cross-linked (314 MPa) versus dry GTA-cross-linked fibers (378 MPa) (Figure 7C). The difference between cross-linkers was greatly enhanced in wet fibers; stress at break of wet EDC-cross-linked fibers (40

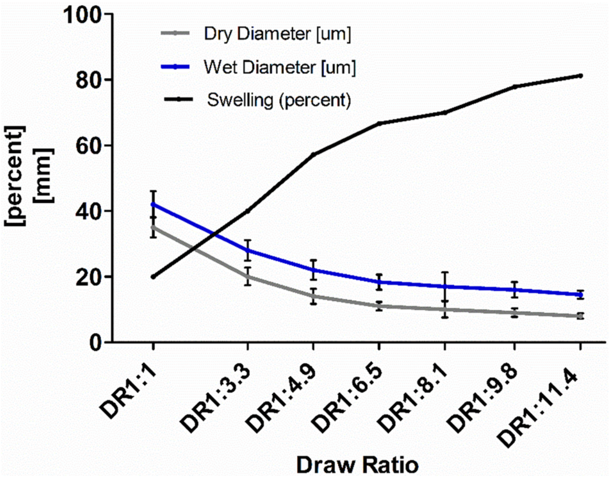

Figure 6. Effect of draw ratio on fiber diameter and swelling. Dry fiber diameter (gray), wet fiber diameter (blue), and the swelling ratio (black) are plotted against the draw ratio. Error bars show the SD.

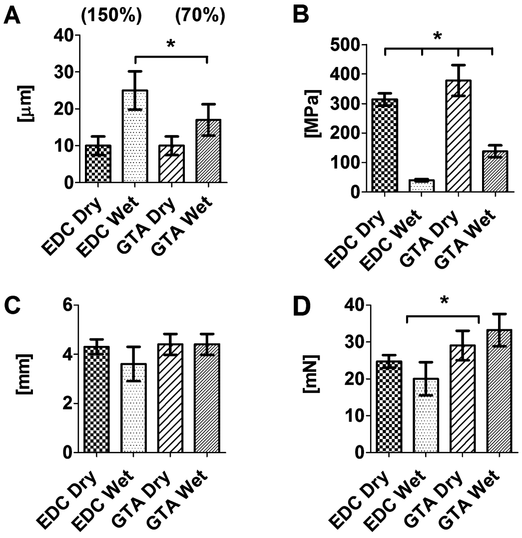

Figure 7. Comparison of the mechanical properties of EDC- versus GTA-cross-linked spun rhcollagen fibers. Fibers were drawn at DR 1:8.1. A − Swelling. The swelling percent for each indicated pair is presented in parentheses. (B) Stress at break. (C) Extension at break. (D) Load at break. Error bars in all graphs denote SD. Asterisks denote the statistical significance of $p < 0.01$.

MPa) was approximately 250% lower than that of wet GTA-cross-linked fibers (138 MPa). The measured load at break was not different for dry versus hydrated fibers cross-linked with identical reagents (Figure 7D), but GTA-cross-linked fibers broke under a higher load than EDC-cross-linked fibers ($P < 0.05$), both in dry and hydrated states.

3.5. Alignment of Rat Tenocytes. To test the effect of draw ratio on cell alignment, rat tenocytes were grown on the EDC-cross-linked fibers. In the control group, the nuclei were generally round in shape and were not oriented in any specific direction (Figure 8A). Undrawn fibers showed a low degree of nuclear orientation, while cell bodies were still amorphous at large. When drawing was introduced, cell bodies and nuclei became elongated and aligned along the fiber axis, which became thinner with increasing draw ratio.

As it has previously been shown that the nucleus is mechanically integrated with the cell body[20] and therefore reflects cell orientation, shape, and configuration,[21] cell alignment was inferred by quantifying the major axis length and orientation of each nucleus. Body shape was not quantified because reliable and repeatable image separation could not be achieved. Figure 8B shows the probability density of the cells' nuclei major axis orientation.

The control cells' nuclear orientation distribution (bottom, red) is rather flat, indicating they are not oriented in any particular direction. Cells cultured on undrawn fibers (DR1:1) show a low degree of nuclear orientation, as visualized by the flattened bell shape curve of their probability density (dark green, second from bottom), centered between 40 and −40°. Upon introduction of drawing (DR 1:3.3), a marked increase in nuclear orientation was observed, with most cells presenting a nuclear orientation between 20° and −20°. When the draw ratio was further increased to DR 1:4.9, a local peak in orientation was seen, followed by a small decline at draw ratios DR 1:6.5 and 1:8.1. Another substantial increase in the nuclear orientation was observed for DR1:9.8 fibers, where the vast majority of nuclei were oriented between 10° and −10°. For technical reasons, the last draw ratio (DR1:11.4) fibers were omitted from this experiment.

Figure 8C presents the length of the cell's nucleus to area ratio. This parameter was used as an indicator of a prolate cell shape, and the division by the area was introduced to reduce the effect of nuclear size variability. The lowest ratio of length to area (reflecting a round shape) was observed among control cells. A strong increase ($P < 0.05$) was noted among cells cultured on undrawn fibers (DR 1:1), followed by an additional increase when drawing was introduced ($P < 0.05$). This trend continued until a local peak was obtained in cultures with DR 1:4.9 fibers. Draw ratios DR 1:6.5 and 1:8.1 showed a small decrease in the length/area ratio, while the largest ratio was obtained from cells grown on fibers with the highest draw ratio (DR 1:9.8).

4. DISCUSSION

4.1. Wet Spinning and Drawing of Rhcollagen. Order and alignment lie at the basis of the molecular structure of high-modulus, high tenacity fibers.[22] The fiber-forming monomers can be roughly divided into two main groups: stiff, interactive molecules and flexible, inert molecules.[22,23] Each group of polymers is spun using different methods that rely on different principles; rigid molecules form a liquid crystalline dope that is aligned by the shear forces applied as it passes through the narrow spinneret, while flexible, inert molecules are spun by methods that rely on extensive drawing to create order. In this work, we have attempted to combine both shear alignment and drawing to order and orient the collagen molecules, which, to the best of our knowledge is the first report of this type in the literature.

We have previously reported the formation of highly aligned and ordered fibers by wet spinning of liquid crystalline rhcollagen dope (at a concentration of 180 mg/mL), without drawing.[24] The shear forces acting on the dope were sufficient to align the monomers in the injection direction, and the order was then preserved upon coagulation. However, working with such concentrated, high viscosity solutions can be very challenging, especially if the goal is to obtain thin fibers (<10 μm). Injection of such dopes through small diameter spinnerets requires high pressures and is accompanied by frequent clogging.

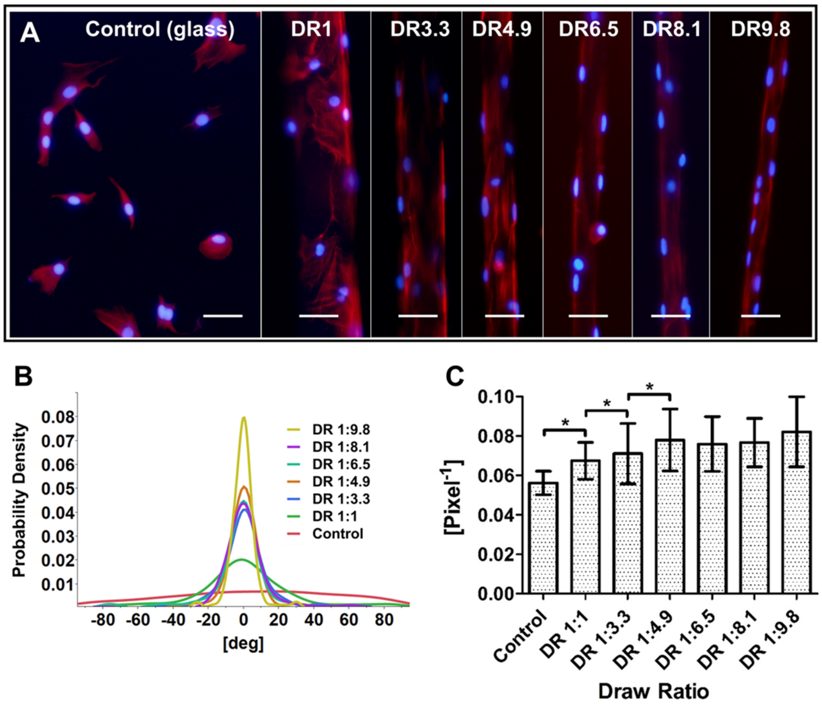

Figure 8. Rat tenocyte alignment on the drawn rhcollagen fibers. (A) Fluorescence microscope images of tenocytes grown on rhcollagen fibers. The DAPI-stained nuclei appear blue, and Pahlloidin-stained actin fibers appear red. The left most image shows tenocytes grown on glass slide as the control. Next to it, from left to right, are images of cells grown on fibers with increasing draw ratios. Scale bar = 50 μm. (B) Nuclear orientation probability density diagram. The nuclear orientation is defined as the angle between the *x*-axis and the major axis of the nucleus. The fiber axis was set parallel to the *x*-axis (0°). (C) Nucleus length to area ratio (in pixels). The number of cells assessed from every experimental group was $n = 206$, 216, 161, 150, 153, 178, and 117, for the control, DR 1:1, DR 1:3.3, DR 1:4.9, DR 1:6.5, DR 1:8.1, and DR 1:9.8, respectively. Error bars show the SD. Asterisks denote the statistical significance of $p < 0.05$.

We therefore decreased the dope concentration to 30 mg/mL, which lowered the viscosity and enabled continuous spinning. This concentration is substantially higher than the concentration reported in most soluble collagen fiber spinning works (1−10 mg/mL[6c,f−i,17,25]) and offers two advantages: first, the formed fiber is solid and strong enough to support its own weight immediately upon exit from the spinneret, allowing high speed spin-drawing without the need for prolonged incubations or cumbersome collection devices. This further allowed efficient decoupling of the spinning operation from downstream stages, such as washing and cross-linking, which can be performed directly on the spool. A flexible, modular spinning process is obtained, that can be adjusted for different cross-linking methods, or accommodate additional buffer incubations (i.e., for fibrillogenesis), when required. The second advantage of concentrated dope spinning is improved fibrillar order and alignment. It has been shown that the degree of orientation induced in isotropic, high aspect ratio mesogen solutions by shear forces is dependent on concentration.[26] Concentrated solutions show increased alignment and orientation compared to that of dilute solutions under similar shear and may even become nematic under certain conditions.[27]

Although spin-drawing is a critical element in both natural spinning mechanisms and modern fiber spinning technologies, and has been used for silk protein[28] and even gelatin[29] fiber spinning methodologies, spin drawing of native, soluble collagen fibers has not been previously reported. Postspin drawing of collagen fibers (i.e., stretching of the previously spun, solid fibers) has been reported[25g−i] and shown to improve alignment and mechanical performance. It is, however, significantly different from spin-drawing, where the liquid dope is drawn directly out of the spinneret and stretched several fold while concomitantly undergoing a sol−gel transition that is induced by drying and neutralization. During this process, the collagen molecules are in a semidissolved state; they are free enough to slide past each other, but stronger interactions gradually develop between them as the pH nears the pI, and water is removed. These intermolecular interactions pull the molecules from both ends in the direction of the fiber axis, aligning and packing them tightly together, until they are solidified in the form of fibrils. In addition to the high levels of density and alignment achieved by spin drawing, it also allows for high spinning rates and the formation of thin fibers. In our experiments, we reached spinning rates of up to 1,000 m/h (for comparison, the highest rate previously reported was 60 m/h[25i]) and fiber diameters as thin as 8 μm (see Table S1).

4.2. Effect of Draw Ratio Rhcollagen Fiber Morphology and Structure. As observed in the SEM images (Figure 2 and Figure 3) and corroborated by the polarized microscopy images (Figure 4), undrawn and low draw ratio fibers display a double layered, core−shell fiber structure. Such a structure is often encountered in wet spinning (PLA,[30] Rayon[31]) and dry jet wet spinning processes (Kevlar[23]). Its formation begins as soon as the liquid dope exits the spinneret into the coagulation bath, where it begins to coagulate and harden on its outer side. A solid and denser external layer is thus formed, acting as a barrier that slows coagulation of the inner material. If drawing is exerted, the take-up forces are borne by this solid layer that is consequently stretched and aligned. The outcome is an aligned, dense outer shell that encompasses a less ordered, less oriented, and less compact core. As the draw ratio increases, the shell becomes more aligned and oriented, and also takes up more of

Table 1. A Summary of the Mechanical Performance (Hydrated) of the Best Performing Collagen Fibers Published over the Last 30 Years

stress at break	modulus	strain at break	cross-linking method	reference
151 ± 31	888 ± 153	20.5 ± 1.95	GTA	current study
110 ± 38	NA	NA	GTA	Dunn et. al.[6i]
93.9 ± 19.2	775 ± 173	14.3 ± 1.9	GTA	Caves et. al.[25i]
91.8 ± 31.4	895 ± 205.9	11.87 ± 1.92	DHT[a]	Wang et. al.[25e]
91.2 ± 10.1	696 ± 38	11 ± 1	NDGA[b]	Koob et. al.[33]
66.2 ± 17.2	407 ± 96.6	16.1 ± 2.7	GTA	Kato et. al.[6h]
57.1 ± 11.82	503.9 ± 101.1	13.8 ± 1.68	DHT[a]	Pins et. al.[25h]
50 ± 13.4	484.7 ± 76.3	NA	EDC	Gentleman et. al.[34]

[a]Dehydrothermal cross-linking for 5 days, at 110 °C. [b]Nordihydroguaiaretic acid.

the fiber cross-section area, until a uniform structure is formed, composed only of a uniform, tightly packed, and aligned material.

The wrinkled and crumpled morphology observed on the outer shell of the undrawn (DR 1:1) fibers may be the result of the shear forces exerted by the coagulant liquid on the external surfaces of the semicoagulated fiber as it is injected into it or the outcome of the spiraling or rolling movement of the free fiber during the coagulation.

The internal fiber core structure displays a wavy crimp pattern, visible in both the SEM and polarized microscope images of the undrawn (DR 1:1) or low draw ratio fibers (DR 1:3.3). Similar patterns are naturally formed by liquid crystalline collagen solutions and have been hypothesized to play a role in the formation of tendon crimp.[32] As the draw ratio increased, the wavy pattern disappeared, perhaps due to the straightening by fiber drawing.

The retardance (Figure 4) and birefringence (Figure S1) of the fibers show an overall increase in the fiber molecular order with increasing draw ratio. Interestingly, a strong local peak was observed for DR1:4.9, indicating increased molecular order for that draw ratio. Although still not well understood, the appearance of a local maxima in the birefringence signal has been previously reported for postspin stretched collagen fibers[25g,h] and silk fibers.[28]

4.3. Mechanical Properties.

The mechanical properties of the fibers presented in this work significantly surpassed those previously reported. A comparison of the hydrated fibers' mechanical properties to literature data of reconstituted collagen fibers (Table 1) indicated an improvement of more than 25% for strain and 30% for UTS.

A comparison between the stress/strain plots of representative hydrated fibers and a hydrated human patellar tendon is presented in Figure 9. Human patellar and Achilles tendons were measured to have a UTS of 81.3 and 60 MPa, strain at break of 0.21 and 0.18, and modulus of 550 and 513 MPa, respectively.[35] The DR 1:9.8, GTA cross-linked fibers displayed a UTS of 150 MPa, a strain at break of 0.21, and a Young's modulus of 890 MPa. The drawn fibers were therefore comparable to natural human tendons in their stress at break but had almost twice the UTS, giving them a substantially higher toughness.

Overall, fiber stress/strain curves corroborated with data obtained from the SAX diffraction profiles and were similar in shape to curves of aligned amorphous material (for an expanded presentation of dry and hydrated fiber stress/strain curves, see Figure S4). Undrawn and low draw ratio fibers displayed a distinct toe region, an integral part of the stress−strain curves of the natural tendon,[36] which is attributed to straightening of the tendon crimp under small strains. It is plausible that the toe region observed here results from the crimp pattern observed in the undrawn/low draw ratio fibers. The general shape of the curves was intermediate between that of rubber and of a semicrystalline polymer above its glass transition, as has been reported before for wet-spun collagen fibers.[6h,25b,e] Fibers spun at high draw ratios more closely resembled semicrystalline polymers, with elevated stress and a more pronounced yield point. The stress/strain curves of the hydrated fibers demonstrated a more "rubbery" behavior, with a flatter curve, lower stress, and a very flat yield point.

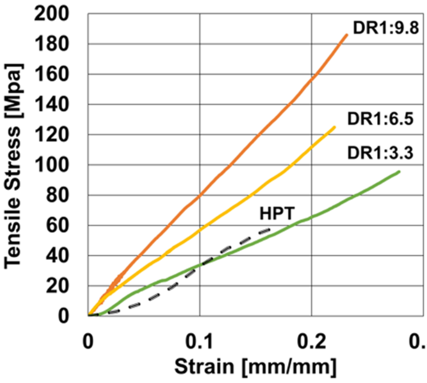

Figure 9. Comparison of stress/strain plots from representative hydrated fibers versus a hydrated human patellar tendon (HPT).[35a] Fiber DRs are noted on the plot.

The mechanical properties of the fibers were greatly affected by the draw ratio. Both the UTS and the modulus significantly increased with the introduction of drawing and continued rising along a steep slope with each increment in the draw ratio (Figure 5A and B). For the dry fibers, peak values of 378 MPa and 3.5 GPa for the UTS and modulus, respectively, were measured at DR 1:8.1, beyond which further drawing did not improve the UTS or modulus. A peak in the UTS at an optimal draw ratio is often observed in drawn polymer fibers, where beyond a threshold value small voids and defects are introduced into the material structure and result in a deterioration of the mechanical performance.[37]

As seen for many polymer fibers, drawing increases alignment, orientation, and crystallinity of the fiber molecular structure, which increases strength and stiffness, but decreases strain and toughness. In contrast to the behavior of most polymers,[37a,38] silk,[28] and postspin collagen,[6d] where extensibility declines with an increase in draw ratio, a peak strain of 0.25 was observed at DR 1:3.3, after which it gradually and linearly declined. A similar observation was noted for postspin draw spider silk,[39] which was hypothesized to be the result of improved molecular interactions between the silk monomers upon stretching. Strain at break and load at break parameters were virtually unchanged by hydration, whereas the UTS and modulus (see Figure S3) were substantially reduced. Taken together, the decline in the UTS and Young's modulus can be attributed mainly to the increase in fiber diameter, i.e., swelling, which appeared to be affected by the draw ratio, with low draw ratio fibers swelling substantially less than high draw ratio fibers. As all the fibers were cross-linked with 0.1% GTA and their melting temperatures were similar, regardless of their draw ratios, it is reasonable to assume that the degree of cross-linking was similar regardless of the draw ratio. The differences in swelling properties can therefore be primarily attributed to the difference in fiber diameter through its impact on surface to volume ratios and diffusion distances.

Comparison of the GTA- versus the EDC-cross-linked fibers showed that when dry, EDC-cross-linked fibers had the same extension and only a slightly reduced load at break as the GTA-cross-linked fibers. However, hydration had a significant impact, with EDC-cross-linked fibers swelling substantially more and displaying notably reduced strength, breaking at 40 MPa versus 138 MPa for fibers cross-linked with GTA.

4.4. Cell Culture. Rat tenocyte alignment on spun rhcollagen fibers demonstrated that the degree of molecular and fibrillar alignment in the fiber shell influences cell shape and directionality, as reflected by the nuclear shape and orientation. Interestingly, cellular alignment and orientation were affected by draw ratio, as predicted by the SAX (Figure S2) and birefringence (Figure S1) measurements, with a strong increase from DR 1:1 to 1:4.9 fibers, followed by a plateau or even a decrease until DR 1:8.1, followed by another strong increase to 9.8. As mentioned above, the reason for the local peak observed in SAX and birefringence measurements at DR 1:4.9 and the decrease that followed it to fibers of DR 1:6.5 and 1:8.1 is unclear. Intuitively, it is anticipated that the degree of order closely matches the mechanical performance and rises linearly with draw ratio. It is interesting therefore that the degree of cell alignment closely followed the pattern detected by the SAX and birefringence measurements.

5. CONCLUSIONS

This work demonstrates that by combination of shear alignment of concentrated collagen dope and spin drawing fibers with diameters of <10 μm can be continuously produced at rates on the order of 1000 m/h, yielding approximately 14 km of fiber per 1 g of collagen. GTA cross-linked fibers displayed a wet strain and UTS that were comparable to and even higher than native human tendons. Rat tenocytes cultured on EDC-cross-linked fibers aligned along the fiber axis indicating that the aligned fibers possess the ability to cue directionality in cells. The spinning technology is simple, can be easily scaled-up, and allows for the introduction of additional incubations and cross-linking methods. We believe that the production of high quantities of thin, strong rhcollagen fibers may lead to significant progress in the field of advanced biotextile-based tissue engineering and regenerative medicine.

■ ASSOCIATED CONTENT

Ⓢ Supporting Information

The Supporting Information is available free of charge on the ACS Publications website at DOI: 10.1021/acsbiomaterials.5b00461.

Plot of the fibers' birefringence versus draw ratio; small angle X-ray scattering analysis of the fibers; comparison of mechanical properties between dry and hydrated fibers; representative dry and hydrated stress−strain plots of fibers spun at different draw ratios; and fiber dimensions and spinning rate (PDF)

■ AUTHOR INFORMATION

Corresponding Author

*Phone: +972-54-2341863. E-mail: Shoseyov@agri.huji.ac.il.

Author Contributions

Y.S., C.T., and U.R. contributed the SAXS figure to this work.

Notes

The authors declare the following competing financial interest(s): Professor Shoseyov is associated with Collplant Ltd. Other authors have no relevant financial interests related to the material in the manuscript.

■ ACKNOWLEDGMENTS

The research was financially supported by the to the Minerva center for bio-hybrid complex systems, the Focal Technology Areas program for Hybrid Nanomaterials and Formulations for Functional Coatings and Printed Devices, and CollPlant Ltd. The authors would like to thank Sigal Roth for her contribution to the development of the presented spinning methodology, and Dr. Tiffany Abitbol for her revision of the manuscript.

■ ABBREVIATIONS

DR, draw ratio; CPD, critical point drying; UTS, ultimate tensile stress; DSC, differential scanning calorimetry; SAX, small angle X-ray scattering; DHT, dehydrothermal cross-linking; NDGA, nordihydroguaiaretic acid

■ REFERENCES

(1) (a) Coburn, J.; Gibson, M.; Bandalini, P. A.; Laird, C.; Mao, H.-Q.; Moroni, L.; Seliktar, D.; Elisseeff, J. Biomimetics of the extracellular matrix: an integrated three-dimensional fiber-hydrogel composite for cartilage tissue engineering. *Smart structures and systems* **2011**, *7* (3), 213. (b) Tamayol, A.; Akbari, M.; Annabi, N.; Paul, A.; Khademhosseini, A.; Juncker, D. Fiber-based tissue engineering: Progress, challenges, and opportunities. *Biotechnol. Adv.* **2013**, *31* (5), 669−687. (c) Murugan, R.; Ramakrishna, S. Nano-featured scaffolds for tissue engineering: a review of spinning methodologies. *Tissue Eng.* **2006**, *12* (3), 435−447.

(2) Van Lieshout, M.; Vaz, C.; Rutten, M.; Peters, G.; Baaijens, F. Electrospinning versus knitting: two scaffolds for tissue engineering of the aortic valve. *J. Biomater. Sci., Polym. Ed.* **2006**, *17* (1−2), 77−89.

(3) Lu, H. H.; Cooper, J. A.; Manuel, S.; Freeman, J. W.; Attawia, M. A.; Ko, F. K.; Laurencin, C. T. Anterior cruciate ligament regeneration using braided biodegradable scaffolds: in vitro optimization studies. *Biomaterials* **2005**, *26* (23), 4805−4816.

(4) Ateshian, G. A. Artificial cartilage: weaving in three dimensions. *Nat. Mater.* **2007**, *6* (2), 89−90.

(5) Mano, J.; Silva, G.; Azevedo, H. S.; Malafaya, P.; Sousa, R.; Silva, S.; Boesel, L.; Oliveira, J. M.; Santos, T.; Marques, A. Natural origin biodegradable systems in tissue engineering and regenerative medicine: present status and some moving trends. *J. R. Soc., Interface* **2007**, *4* (17), 999−1030.

(6) (a) Griset, E. J.; Reissmann, T. L.; Joseph, N. Method of Producing a Collagen Strand. US Patent US14298461A, 1963; (b) Braun, B.; Braun, E. Production of Collagen Strands. US Patent US2747228A, 1956; (c) Goldstein, J. D.; Tria, A.; Zawadsky, J.; Kato, Y.; Christiansen, D.; Silver, F. Development of a reconstituted collagen tendon prosthesis. *J. Bone Joint Surg. Am.* **1989**, *71*, 1183−1191.

(d) Pins, G. D.; Silver, F. H. A self-assembled collagen scaffold suitable for use in soft and hard tissue replacement. *Mater. Sci. Eng., C* **1995**, *3* (2), 101−107. (e) Meyer, M.; Baltzer, H.; Schwikal, K. Collagen fibres by thermoplastic and wet spinning. *Mater. Sci. Eng., C* **2010**, *30* (8), 1266−1271. (f) Zeugolis, D.; Paul, R.; Attenburrow, G. Extruded collagen fibres for tissue-engineering applications: influence of collagen concentration and NaCl amount. *J. Biomater. Sci., Polym. Ed.* **2009**, *20* (2), 219−234. (g) Zeugolis, D.; Paul, R.; Attenburrow, G. Post-self-assembly experimentation on extruded collagen fibres for tissue engineering applications. *Acta Biomater.* **2008**, *4* (6), 1646−1656. (h) Kato, Y. P.; Christiansen, D. L.; Hahn, R. A.; Shieh, S. J.; Goldstein, J. D.; Silver, F. H. Mechanical properties of collagen fibres: a comparison of reconstituted and rat tail tendon fibres. *Biomaterials* **1989**, *10* (1), 38−42. (i) Dunn, M. G.; Avasarala, P. N.; Zawadsky, J. P. Optimization of extruded collagen fibers for ACL reconstruction. *J. Biomed. Mater. Res.* **1993**, *27* (12), 1545−1552. (j) Enea, D.; Henson, F.; Kew, S.; Wardale, J.; Getgood, A.; Brooks, R.; Rushton, N. Extruded collagen fibres for tissue engineering applications: effect of crosslinking method on mechanical and biological properties. *J. Mater. Sci.: Mater. Med.* **2011**, *22* (6), 1569−1578.

(7) (a) Vollrath, F.; Knight, D. P. Liquid crystalline spinning of spider silk. *Nature* **2001**, *410* (6828), 541−8. (b) Lazaris, A.; Arcidiacono, S.; Huang, Y.; Zhou, J.-F.; Duguay, F.; Chretien, N.; Welsh, E. A.; Soares, J. W.; Karatzas, C. N. Spider silk fibers spun from soluble recombinant silk produced in mammalian cells. *Science* **2002**, *295* (5554), 472−476. (c) Vollrath, F.; Knight, D.; Hu, X. Silk production in a spider involves acid bath treatment. *Proc. R. Soc. London, Ser. B* **1998**, *265* (1398), 817−820. (d) Knight, D.; Vollrath, F. Liquid crystals and flow elongation in a spider's silk production line. *Proc. R. Soc. London, Ser. B* **1999**, *266* (1418), 519−523.

(8) Shen, Y.; Johnson, M. A.; Martin, D. C. Microstructural characterization of Bombyx mori silk fibers. *Macromolecules* **1998**, *31* (25), 8857−8864.

(9) (a) Knight, D. P.; Hunt, S. Fine structure of the dogfish egg case: a unique collagenous material. *Tissue Cell* **1976**, *8* (1), 183−193. (b) Knight, D. P.; Feng, D.; Stewart, M. Structure and function of the salachian egg case. *Biological Reviews* **1996**, *71* (1), 81−111. (c) Luong, T.-T.; Boutillon, M.-M.; Garrone, R.; Knight, D. P. Characterization of Selachian Egg Case Collagen. *Biochem. Biophys. Res. Commun.* **1998**, *250* (3), 657−663. (d) Knupp, C.; Chew, M.; Squire, J. Collagen packing in the dogfish egg case wall. *J. Struct. Biol.* **1998**, *122* (1), 101−110.

(10) (a) Harrington, M. J.; Waite, J. H. pH-dependent locking of giant mesogens in fibers drawn from mussel byssal collagens. *Biomacromolecules* **2008**, *9* (5), 1480−1486. (b) Harrington, M. J.; Waite, J. H. How nature modulates a fiber's mechanical properties: mechanically distinct fibers drawn from natural mesogenic block copolymer variants. *Adv. Mater.* **2009**, *21* (4), 440−444. (c) Hassenkam, T.; Gutsmann, T.; Hansma, P.; Sagert, J.; Waite, J. H. Giant bent-core mesogens in the thread forming process of marine mussels. *Biomacromolecules* **2004**, *5* (4), 1351−1355.

(11) Ebrahimi, D.; Tokareva, O.; Rim, N.; Wong, J. Y.; Kaplan, D. L.; Buehler, M. J. Silk−its mysteries, how it's made, and how it's used. *ACS Biomater. Sci. Eng.* **2015**, *1*, 864.

(12) Stein, H.; Wilensky, M.; Tsafrir, Y.; Rosenthal, M.; Amir, R.; Avraham, T.; Ofir, K.; Dgany, O.; Yayon, A.; Shoseyov, O. Production of bioactive, post-translationally modified, heterotrimeric, human recombinant type-I collagen in transgenic tobacco. *Biomacromolecules* **2009**, *10* (9), 2640−5.

(13) Eder, M.; Lütz-Meindl, U.; Weiss, I. M. Non-invasive LC-PolScope imaging of biominerals and cell wall anisotropy changes. *Protoplasma* **2010**, *246* (1−4), 49−64.

(14) Pufe, T.; Petersen, W.; Tillmann, B.; Mentlein, R. The angiogenic peptide vascular endothelial growth factor is expressed in foetal and ruptured tendons. *Virchows Arch.* **2001**, *439* (4), 579−585.

(15) (a) Carpenter, A. E.; Jones, T. R.; Lamprecht, M. R.; Clarke, C.; Kang, I. H.; Friman, O.; Guertin, D. A.; Chang, J. H.; Lindquist, R. A.; Moffat, J.; Golland, P.; Sabatini, D. M. CellProfiler: image analysis software for identifying and quantifying cell phenotypes. *Genome Biol.* **2006**, *7* (10), R100. (b) CellProfiler. www.cellprofiler.org.

(16) (a) Whittaker, P.; Canham, P. B. Demonstration of quantitative fabric analysis of tendon collagen using two-dimensional polarized light microscopy. *Matrix* **1991**, *11* (1), 56−62. (b) Bromage, T. G.; Goldman, H. M.; McFarlin, S. C.; Warshaw, J.; Boyde, A.; Riggs, C. M. Circularly polarized light standards for investigations of collagen fiber orientation in bone. *Anat. Rec.* **2003**, *274B* (1), 157−168. (c) Wolman, M.; Kasten, F. Polarized light microscopy in the study of the molecular structure of collagen and reticulin. *Histochemistry* **1986**, *85* (1), 41−49. (d) Nieminen, M. T.; Rieppo, J.; Töyräs, J.; Hakumäki, J. M.; Silvennoinen, J.; Hyttinen, M. M.; Helminen, H. J.; Jurvelin, J. S. T2 relaxation reveals spatial collagen architecture in articular cartilage: a comparative quantitative MRI and polarized light microscopic study. *Magn. Reson. Med.* **2001**, *46* (3), 487−493.

(17) Kato, Y. P.; Silver, F. H. Formation of continuous collagen fibres: evaluation of biocompatibilily and mechanical properties. *Biomaterials* **1990**, *11* (3), 169−175.

(18) (a) Huang-Lee, L. L.; Cheung, D. T.; Nimni, M. E. Biochemical changes and cytotoxicity associated with the degradation of polymeric glutaraldehyde derived crosslinks. *J. Biomed. Mater. Res.* **1990**, *24* (9), 1185−1201. (b) Gough, J. E.; Scotchford, C. A.; Downes, S. Cytotoxicity of glutaraldehyde crosslinked collagen/poly (vinyl alcohol) films is by the mechanism of apoptosis. *J. Biomed. Mater. Res.* **2002**, *61* (1), 121−130.

(19) Fagerholm, P.; Lagali, N. S.; Ong, J. A.; Merrett, K.; Jackson, W. B.; Polarek, J. W.; Suuronen, E. J.; Liu, Y.; Brunette, I.; Griffith, M. Stable corneal regeneration four years after implantation of a cell-free recombinant human collagen scaffold. *Biomaterials* **2014**, *35* (8), 2420−2427.

(20) Maniotis, A. J.; Chen, C. S.; Ingber, D. E. Demonstration of mechanical connections between integrins, cytoskeletal filaments, and nucleoplasm that stabilize nuclear structure. *Proc. Natl. Acad. Sci. U. S. A.* **1997**, *94* (3), 849−854.

(21) (a) Dalby, M. J.; Riehle, M. O.; Yarwood, S. J.; Wilkinson, C. D.; Curtis, A. S. Nucleus alignment and cell signaling in fibroblasts: response to a micro-grooved topography. *Exp. Cell Res.* **2003**, *284* (2), 272−280. (b) Xue, N.; Li, X.; Bertulli, C.; Li, Z.; Patharagulpong, A.; Sadok, A.; Huang, Y. Rapid Patterning of 1-D Collagenous Topography as an ECM Protein Fibril Platform for Image Cytometry. *PLoS One* **2014**, *9* (4), e93590.

(22) Hearle, J. W. *High-Performance Fibres*. Elsevier: New York, 2001.

(23) Ahmed, D.; Hongpeng, Z.; Haijuan, K.; Jing, L.; Yu, M.; Muhuo, Y. Microstructural developments of poly (p-phenylene terephthalamide) fibers during heat treatment process: a review. *Mater. Res.* **2014**, *17* (5), 1180.

(24) Yaari, A.; Posen, Y.; Shoseyov, O. Liquid crystalline human recombinant collagen: the challenge and the opportunity. *Tissue Eng., Part A* **2013**, *19* (13−14), 1502−1506.

(25) (a) Fofonoff, T. W.; Bell, E., Apparatus and method for spinning and processing collagen fiber. Us Patent US5851290A, 1996; (b) Zeugolis, D. I.; Paul, G. R.; Attenburrow, G. Cross-linking of extruded collagen fibers—A biomimetic three-dimensional scaffold for tissue engineering applications. *J. Biomed. Mater. Res., Part A* **2009**, *89A* (4), 895−908. (c) Kato, Y. P.; Dunn, M.; Zawadsky, J. P.; Tria, A.; Silver, F. Regeneration of Achilles tendon with a collagen tendon prosthesis. Results of a one-year implantation study. *J. Bone Joint Surg.* **1991**, 73 (4), 561−574. (d) Kato, Y. P.; Silver, F. H. In *Properties of manually produced and automated continuous collagen fibers*, Engineering in Medicine and Biology Society, 1989. Images of the Twenty-First Century., Proceedings of the Annual International Conference of the IEEE Engineering in, IEEE: 1989; pp 843−844;. (e) Ming-Che, W.; Pins, G. D.; Silver, F. H. Collagen fibres with improved strength for the repair of soft tissue injuries. *Biomaterials* **1994**, *15* (7), 507−512. (f) Zeugolis, D. I.; Paul, R. G.; Attenburrow, G. Factors influencing the properties of reconstituted collagen fibers prior to self-assembly: animal species and collagen extraction method. *J. Biomed. Mater. Res., Part A* **2008**, *86A* (4), 892−904. (g) Pins, G. D.; Huang, E. K.; Christiansen, D. L.; Silver, F. H. Effects of static axial strain on the

tensile properties and failure mechanisms of self-assembled collagen fibers. *J. Appl. Polym. Sci.* **1997**, *63* (11), 1429−1440. (h) Pins, G. D.; Christiansen, D. L.; Patel, R.; Silver, F. H. Self-assembly of collagen fibers. Influence of fibrillar alignment and decorin on mechanical properties. *Biophys. J.* **1997**, *73* (4), 2164−2172. (i) Caves, J. M.; Kumar, V. A.; Wen, J.; Cui, W.; Martinez, A.; Apkarian, R.; Coats, J. E.; Berland, K.; Chaikof, E. L. Fibrillogenesis in continuously spun synthetic collagen fiber. *J. Biomed. Mater. Res., Part B* **2010**, *93B* (1), 24−38. (j) Siriwardane, M. L.; DeRosa, K.; Collins, G.; Pfister, B. J. Controlled formation of cross-linked collagen fibers for neural tissue engineering applications. *Biofabrication* **2014**, *6* (1), 015012. (k) Cavallaro, J. F.; Kemp, P. D.; Kraus, K. H. Collagen fabrics as biomaterials. *Biotechnol. Bioeng.* **1994**, *43* (8), 781−791.

(26) (a) Pope, D.; Keller, A. Alignment of macromolecules in solution by elongational flow; a study of the effect of pure shear in a four roll mill. *Colloid Polym. Sci.* **1977**, *255* (7), 633−643. (b) Lenstra, T.; Dogic, Z.; Dhont, J. Shear-induced displacement of isotropic-nematic spinodals. *J. Chem. Phys.* **2001**, *114* (22), 10151−10162.

(27) Schmitt, V.; Lequeux, F.; Pousse, A.; Roux, D. Flow behavior and shear induced transition near an isotropic/nematic transition in equilibrium polymers. *Langmuir* **1994**, *10* (3), 955−961.

(28) Um, I. C.; Ki, C. S.; Kweon, H.; Lee, K. G.; Ihm, D. W.; Park, Y. H. Wet spinning of silk polymer: II. Effect of drawing on the structural characteristics and properties of filament. *Int. J. Biol. Macromol.* **2004**, *34* (1), 107−119.

(29) Fukae, R.; Maekawa, A.; Sangen, O. Gel-spinning and drawing of gelatin. *Polymer* **2005**, *46* (25), 11193−11194.

(30) Nelson, K. D.; Romero, A.; Waggoner, P.; Crow, B.; Borneman, A.; Smith, G. M. Technique paper for wet-spinning poly (L-lactic acid) and poly (DL-lactide-co-glycolide) monofilament fibers. *Tissue Eng.* **2003**, *9* (6), 1323−1330.

(31) (a) Müller, M.; Riekel, C.; Vuong, R.; Chanzy, H. Skin/core micro-structure in viscose rayon fibres analysed by X-ray microbeam and electron diffraction mapping. *Polymer* **2000**, *41* (7), 2627−2632. (b) Morehead, F. F.; Sisson, W. A. Skin effect in viscose rayon. *Text. Res. J.* **1945**, *15* (12), 443−450.

(32) (a) Giraud-Guille, M. M.; Besseau, L.; Martin, R. Liquid crystalline assemblies of collagen in bone and in vitro systems. *J. Biomech* **2003**, *36* (10), 1571−9. (b) Giraud-Guille, M. M. Liquid crystallinity in condensed type I collagen solutions. A clue to the packing of collagen in extracellular matrices. *J. Mol. Biol.* **1992**, *224* (3), 861−73.

(33) Koob, T. J.; Hernandez, D. J. Material properties of polymerized NDGA−collagen composite fibers: development of biologically based tendon constructs. *Biomaterials* **2002**, *23* (1), 203−212.

(34) Gentleman, E.; Lay, A. N.; Dickerson, D. A.; Nauman, E. A.; Livesay, G. A.; Dee, K. C. Mechanical characterization of collagen fibers and scaffolds for tissue engineering. *Biomaterials* **2003**, *24* (21), 3805−3813.

(35) (a) Hashemi, J.; Chandrashekar, N.; Slauterbeck, J. The mechanical properties of the human patellar tendon are correlated to its mass density and are independent of sex. *Clinical Biomechanics* **2005**, *20* (6), 645−652. (b) Lewis, G.; Shaw, K. M. Tensile properties of human tendo Achillis: effect of donor age and strain rate. *Journal of foot and ankle surgery* **1997**, *36* (6), 435−445.

(36) (a) Kastelic, J.; Palley, I.; Baer, E. A structural mechanical model for tendon crimping. *J. Biomech.* **1980**, *13* (10), 887−893. (b) Freed, A. D.; Doehring, T. C. Elastic model for crimped collagen fibrils. *J. Biomech. Eng.* **2005**, *127* (4), 587−593. (c) Fratzl, P.; Misof, K.; Zizak, I.; Rapp, G.; Amenitsch, H.; Bernstorff, S. Fibrillar structure and mechanical properties of collagen. *J. Struct. Biol.* **1998**, *122* (1−2), 119−22.

(37) (a) Gupta, B.; Revagade, N.; Anjum, N.; Atthoff, B.; Hilborn, J. Preparation of poly (lactic acid) fiber by dry-jet-wet-spinning. I. Influence of draw ratio on fiber properties. *J. Appl. Polym. Sci.* **2006**, *100* (2), 1239−1246. (b) Sawai, D.; Fujii, Y.; Kanamoto, T. Development of oriented morphology and tensile properties upon superdawing of solution-spun fibers of ultra-high molecular weight poly (acrylonitrile). *Polymer* **2006**, *47* (12), 4445−4453. (c) Jarecki, L.; Meier, D. J. Ultra-high modulus polyethylene. 1 Effect of drawing temperature. *Polymer* **1979**, *20* (9), 1078−1082. (d) Jayanarayanan, K.; Jose, T.; Thomas, S.; Joseph, K. Effect of draw ratio on the microstructure, thermal, tensile and dynamic rheological properties of insitu microfibrillar composites. *Eur. Polym. J.* **2009**, *45* (6), 1738−1747.

(38) Smith, P.; Lemstra, P. J. Ultra-high-strength polyethylene filaments by solution spinning/drawing. *J. Mater. Sci.* **1980**, *15* (2), 505−514.

(39) Albertson, A. E.; Teulé, F.; Weber, W.; Yarger, J. L.; Lewis, R. V. Effects of different post-spin stretching conditions on the mechanical properties of synthetic spider silk fibers. *Journal of the mechanical behavior of biomedical materials* **2014**, *29*, 225−234.